At-wavelength detection of extreme ultraviolet lithography mask blank defects

Seongtae Jeong and Mourad Idir[a)]
Center for X-ray Optics, Lawrence Berkeley National Laboratory, Berkeley, California 94720

Yun Lin
EECS Department, University of California, Berkeley, California 94720

Lewis Johnson, Seno Rekawa, Michael Jones, Paul Denham, and Phil Batson
Center for X-ray Optics, Lawrence Berkeley National Laboratory, Berkeley, California 94720

Rick Levesque and Patrick Kearney
Lawrence Livermore National Laboratory, Livermore, California 94550

Pei-Yang Yan
Intel Corporation, Santa Clara, California 95052

Eric Gullikson, James H. Underwood, and Jeffrey Bokor[b)]
Center for X-ray Optics, Lawrence Berkeley National Laboratory, Berkeley, California 94720

(Received 29 May 1998; accepted 16 September 1998)

We report the design and operation of an at-wavelength system for extreme ultraviolet lithography mask blank defect detection. Initial results demonstrate sensitivity to submicron size phase defects. The performance of the system is compared with the practical requirements for a mask blank inspection system in terms of the sensitivity and scanning time. © *1998 American Vacuum Society.* [S0734-211X(98)11306-9]

I. INTRODUCTION

Extreme ultraviolet lithography (EUVL) is a promising technology for integrated circuit fabrication for feature sizes less than 0.1 μm.[1,2] It is an optical projection lithography scheme using 13 nm radiation with all-reflective optics based on Mo/Si or Mo/Be multilayer coatings. An EUVL reticle is also reflective, consisting of a multilayer coated substrate and a patterned absorber layer. In order to insure the integrity of the printed pattern, the reticle has to be free of any critical defect which can occur either on the absorber pattern or on the mask blank itself. While several techniques have been proposed for correcting defects in the absorber overlayer pattern, there is no known repair technology for defects in the multilayer coating. Moreover, the defects in the multilayer coating have been shown to be more detrimental than absorber defects of the same dimension and those defects may be very hard to detect.[3] From a recent defect printability study by Lin and Bokor,[4] an opaque defect in the mask blank as small as 40 nm can produce a non-negligible process window reduction for a 0.1 μm contact hole. Therefore, the ability to produce EUVL mask blanks with low defect density is an important technical issue.

Production of a virtually defect-free mask blank requires both a low defect deposition technique and the ability to inspect mask blanks. While the development of a deposition technique for producing a mask blank with low defect density is being actively pursued,[5] the capability for its inspection is not well established. Because the EUVL mask is a reflective mask typically on a silicon substrate, most of the current wafer inspection tools can be employed for the mask blank inspection. These tools include scanning electron microscopy, atomic force microscopy, and laser-based particle detection. However, it is not clear whether these techniques can detect all the relevant printable defects, especially the defects deeply buried in or below the multilayer coating. These probes tend to have a limited probing depth into the multilayer coating and correlations between the EUV response and the probing capability of these tools are not well established. Therefore, an at-wavelength inspection system is essential to capture all the relevant multilayer defects as a defect learning tool at least during the developmental stage of the low defect mask blank. Furthermore, an at-wavelength inspection system will be useful to study the correlations between the EUV response and current ''non-at-wavelength'' inspection techniques and is expected to assist in establishing proper capability for non-at-wavelength inspection.

In this article, we report on the design and preliminary experimental results of a prototype at-wavelength EUVL mask blank inspection system based on scanning of a focused EUV beam. The initial experimental results on a programmed defect mask blank will be presented and the performance of this prototype system will be evaluated in terms of the actual mask blank inspection requirements.

II. EXPERIMENT

The conceptual idea behind the current inspection system is shown in the inset of Fig. 1. It is somewhat similar to

[a)]Also at: Laboratoire pour l'Utilisation du Rayonnement Electromagnetique, Batiment 209 D Universite Paris SUD 91405 Orsay, France.
[b)]Also at: EECS Department, University of California, Berkeley, California 94720; electronic mail: jbokor@eecs.berkeley.edu

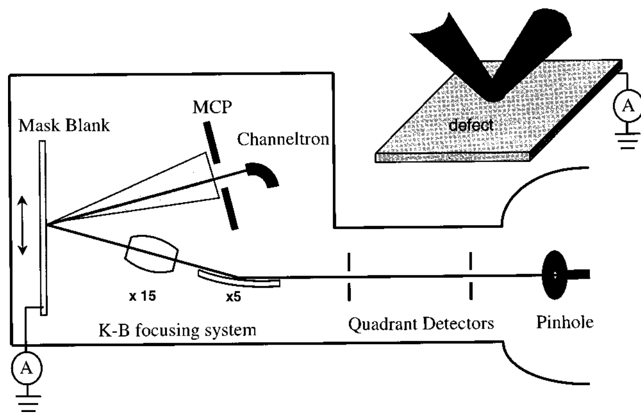

FIG. 1. (Inset) concept behind the instrument. Schematic of the instrument.

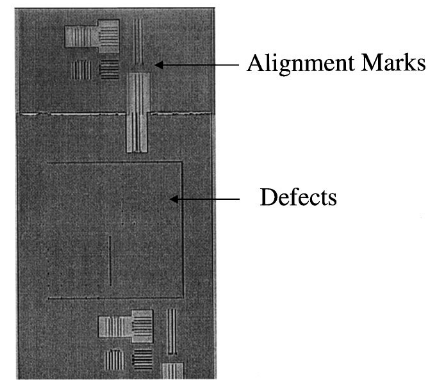

FIG. 2. Optical micrograph of the photoresist pattern of the programmed defect mask.

visible laser-based particulate detection systems. When a focused beam of wavelength 13 nm is incident on the defective region of a mask blank, three possible phenomena can occur. The defect will induce an intensity reduction in the specularly reflected beam, scatter incoming photons into an off-specular direction, and change the amplitude and phase of the electric field at the surface which can be monitored through the change in the photoemission current.[6] The magnitude of these changes will depend on the incident beam size, and the nature, extent, and size of the defect. Inspection of the mask blank is performed by scanning the mask blank with 13 nm light focused to a spot a few micrometers in diameter, while measuring the reflected beam intensity (bright field detection), the scattered beam intensity (dark field detection), and/or the change in the photoemission current.

The schematic layout of the prototype at-wavelength inspection system is shown in Fig. 1. The inspection system is enclosed in a vacuum chamber operating in 10^{-6} Torr and is mounted in series with the reflectometer chamber on the existing beamline 6.3.2 of the advanced light source (ALS) at Lawrence Berkeley National Laboratory (LBNL).[7] The sample is kinematically mounted on an $X-Y$ linear stage with 150 mm travel in either direction allowing a scan of a full 150 mm wafer coated with multilayer. Each axis of the stage is driven by a direct current servo motor with positioning accuracy better than 1 μm. The small spot of EUV light is achieved by demagnifying an illuminated pinhole with a glancing incidence optical system consisting of two mirrors arranged in the Kirkpatrick–Baez (KB)[8] configuration. To eliminate spherical aberration and achieve optimum on-axis image quality each mirror must have the form of an elliptic cylinder. This figure was achieved by a bending method[9] in which a strip mirror is bent by a combination of unequal end couples to approximate an ellipse. A more accurate elliptical figure is achieved through a longitudinal variation of the width of the mirror to vary the local cross-sectional moment of inertia and hence the local curvature.

For the early experiments reported in this article, the focusing system is designed to demagnify a 25 μm pinhole placed at the object plane of the KB optics. With a demagnification factor of 15 in the horizontal plane and 5 in the vertical plane, the optics should thus provide a 1.7×5 μm spot on the mask blank located at the image plane of the KB system. The approximate size and shape of the focused beam is monitored by observing, with a microscope, the fluorescence of a yttrium–aluminum–garnet crystal situated at the sample plane. Its size in orthogonal directions, measured using a knife edge scan, was conservatively estimated to be 4×6 μm full width at half maximum. Several factors contribute to make the observed spot size larger than the geometrical prediction. These include: Imperfections of the mirrors and the bending mechanism, and alignment errors of the optical elements.

The focused beam is incident on the sample with an angle of 9° off normal and the reflected beam and the scattered photons are detected by the detector assembly which is located 15 cm away from the sample. The detector assembly consists of a channeltron electron multiplier for the bright field measurement and a microchannel plate for the dark field detection. The microchannel plate has a hole at the center in order for the specularly reflected beam to be detected by the channeltron detector situated behind the microchannel plate. The channeltron detector can deliver up to 10^7 gain at 2700 V bias voltage with a good linearity and has been measured to deliver shot-noise limited performance even in an analog current output mode. The output of the channeltron was read through a current amplifier. For a higher-rate data acquisition which is essential for a high-throughput inspection system, the data was taken while continuously moving the motor and polling the motor position instead of taking data while the motor is stationary at a specified position. Data acquisition rates of several kilohertz are achievable with this scheme. The whole system is controlled through a motor control unit and analog-to-digital converter module in a VXI crate with a computer.

The alignment of the chamber with respect to the beam is accomplished by a ''beam sight'' consisting of two quadrant detectors separated by 25 cm. Each of the quadrant detectors is composed of four independent detectors surrounding a central opening. The two quad detectors and KB mirror system have been prealigned outside the chamber. For the

TABLE I. Programmed defect size (units: μm).

	Column 1	Column 2	Column 3	Column 4	Column 5
Row 5	8×0.2	4×0.2	2×0.2	0.5×0.2	0.2×0.2
Row 4	8×0.5	4×0.5	2×0.5	0.8×0.5	0.5×0.5
Row 3	8×0.8	4×0.8	2×0.8	1.1×0.8	0.8×0.8
Row 2	8×1.1	4×1.1	2×1.1	1.5×1.1	1.1×1.1
Row 1	8×1.5	4×1.5	3×1.5	2.0×1.5	1.5×1.5

chamber alignment with respect to the incoming EUV beam, the photoemission current on each of the four detectors is monitored and the six-strut system (not shown in Fig. 1) is adjusted until the photocurrent is balanced in both the horizontal detectors and vertical detectors.

As an initial proof-of-principle experiment, a test mask blank with programmed defects of known size and location was scanned to quantify the performance of the current inspection system. This programmed defect mask was patterned on a 150 mm silicon wafer by etching the substrate to produce a relief pattern of small bumps which simulate phase defects. The resist layout is shown in Fig. 2. The etch depth surrounding the alignment marks is 100 nm while the region surrounding the programmed defects was etched 25 nm deep. After the substrate etch step, the Si/Mo multilayer was deposited by the ion beam sputtering deposition developed for low defect density Si/Mo coating.[5] Therefore, the Si/Mo multilayer coating over the unetched region is 25 nm high compared to the surrounding region and acts as a phase defect with a phase error of 7.7π. There is a five row and five column array of rectangular programmed phase defects. The size of the defects varies from 8×1.5 μm to 0.2×0.2 μm as shown in Table I. The spacing between defects is 80 μm in either direction. The scanning wavelength is 13.2 nm with an estimated fractional bandwidth of 1/3000. Only the bright field signal was collected for the experiments reported in this article.

Figure 3(a) is a gray-scale image of a two-dimensional bright field scan of the alignment marks with the pixel size of 10×10 μm. The reflectivity of the bright region was separately measured to be 61.8%. The dark region surrounding the alignment marks shows approximately 30% lower reflectivity relative to the bright region. This reduction in reflectivity occurs uniformly over the bandwidth of the given multilayer. Since these two regions have different etch depths as described in the previous paragraph, the reduction in reflectivity is likely due to the roughening of the substrate during the etch step, thus increasing scattering. The features that appear as lines are actually series of squares of size ranging from 3 to 4 μm. The spacing between the squares varies from 6 to 8 μm. Individual squares are not resolved in these early experiments due to the finite pixel size but each linear chain of squares which are 20 μm apart from each other is clearly resolved. The wavy appearance of the line was traced to a systematic error in the motor drive, which has since been corrected.

Figure 4(a) shows a scan over the region containing programmed defects. The pixel size was 3 μm by 5 μm and the dwell time per pixel was 50 ms. The total scan time for Fig. 4(a) was 6 min. The regularly spaced dark dots are programmed defects showing reduced reflectivity in the bright field. In the bottom row, five programmed defects are clearly observed. Figure 4(c) is the plot of the reflectivity reduction through each row of programmed defects. In topmost line scan, the smallest detected defect has the dimension of 0.5 μm by 0.8 μm as is indicated in the Table I. The 0.5 μm by 0.8 μm phase defect shows a reflectivity reduction greater than the background fluctuation which was approximately 1%. This background fluctuation is mainly due to the shot-noise fluctuation according to the estimated number of detected photons per pixel. There are vertical streaks observed around the programmed defect region and these are due to the tail of the focused EUV spot which arises from residual spherical aberration of the KB optics. A magnified image of the leftmost programmed defect in the bottom row, as shown in Fig. 4(b), reveals the vertical streak more clearly. One interesting observation is that several ''real'' defects were observed in the scanned image of the test mask in addition to the programmed defects. One of them is shown at the bottom of Fig. 4(a). These real defects are quite likely to be a particulate contamination incurred during handling of the mask blank in a nonclean environment. A clean and low particulate environment is essential for counting defects on an EUVL mask blank and providing a meaningful number for the defect density. Efforts such as improving the mask han-

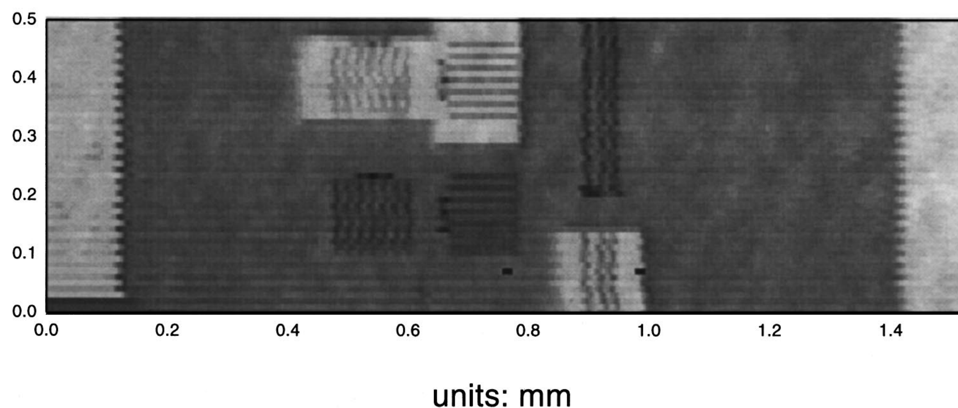

FIG. 3. Bright field scan through the alignment marks. The pixel size is 10×10 μm.

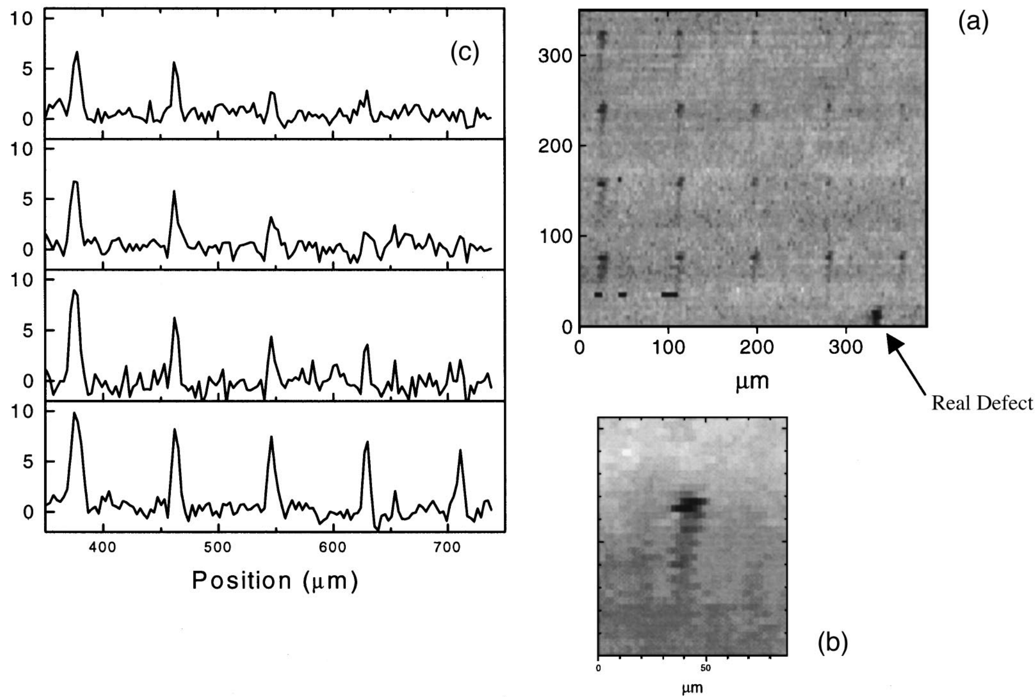

FIG. 4. (a) Gray-scale image of 2D programmed defect mask with pixel size of 3×5 μm. (b) Magnified image of the leftmost defect of the bottom row with pixel size of 2×3 μm. (c) Reflectivity reduction along the programmed defects. Vertical unit is percent.

dling protocol and creating a clean minienvironment to reduce the particulate contamination are currently underway.

Figure 4(c) shows the corresponding reflectivity reduction along the lines containing the defects. The leftmost peak of each row has wider width than the rest in the same row. This is due to the fact that the horizontal dimension of the leftmost defect is greater than that of the focused beam. Despite a factor of 4 difference in area between the leftmost defect and the right most defect of the bottom row, the peak reflectivity reduction does not scale accordingly. This is typical of phase defects for which the reflectivity reduction depends not only on the size of the defect but also on the geometry of the defect with respect to the beam size in a rather complicated fashion. This is because the bright field intensity depends on the *relative* phase variation within the spot. For instance, with a spot of 1 μm diam, either a 10 nm square phase defect or a 2 μm square phase defect would be expected to induce a relatively small bright field reduction as compared with a 0.2 μm square phase defect. This is because, in the first two cases, the relative phase across most of the spot is more uniform than in the last case, in which there is more relative phase variation over the area of the spot.

III. DISCUSSION

In order for an inspection system to be useful, the sensitivity is a critical issue along with the ability to scan a statistically meaningful area of the sample. Given that the estimated size of the critical defect is smaller than 100 nm,[4] a useful inspection system must be sensitive to defects of comparable dimension. The sensitivity of our prototype at-wavelength inspection system critically depends on the focal spot size. According to simple diffraction calculation, with a 1 μm beam spot size, a 100 nm opaque defect is estimated to result in 2.5% reduction in the bright field signal which is readily measurable. The KB mirror system is currently being improved to achieve a smaller spot size. A smaller beam size is also essential to decrease the total scan time. The total amount of time to scan a certain area is determined by the dwell time per pixel multiplied by the number of pixels necessary to cover the area. It is straightforward to understand that the number of pixels to cover the given area scales inversely with the beam area. However, the reflectivity reduction in the bright field scales approximately linearly with the ratio of the defect area to the beam area. Hence, the dwell time to achieve a given signal-to-noise-ratio is shorter with smaller beam size. Because the dominant noise source is expected to be the shot-noise fluctuation of the incoming photons, which varies as the inverse square root of the number of photons per pixel, the dwell time per pixel to achieve the same signal-to-noise ratio decreases as the square of the beam area. Therefore, the total scan time scales approximately with the beam spot area.

While the spot size is an important system parameter in determining the sensitivity and the scan time, there are several paths to decrease the scan time by detecting as many photons as possible. One is to increase the quantum efficiency of the detector by making use of a different coating. The current channletron detector has an estimated quantum efficiency of 7% at 95 eV. Coatings such as MgF_2 have been shown to increase the quantum efficiency to above 20% and to be stable in a high vacuum.[10] An additional path to increase the flux involves reducing the resolving power of the

monochromator. The current resolving power of the monochromator on the 6.3.2 beamline is approximately 3000 with a 50 μm exit slit width. This resolving power is unnecessarily high considering that the typical fractional bandwidth of the multilayer is greater than 1/100. Methods of reducing the resolving power of the beamline will be incorporated into the dedicated beamline for EUVL mask inspection which is under current development and planned for operation in Fall 1998.

IV. CONCLUSION

In this article, successful operation of a prototype at-wavelength mask blank inspection system based on a scanning microfocused EUV beam is reported. From initial scans on a programmed phase defect mask, the current system is shown to be sensitive to phase defects down to 0.5 μm by 0.8 μm with a beam size 4 μm$\times$6 μm. Currently, improvements to the beam spot size are being actively pursued to achieve an EUV beam spot with $\sim$1 μm diam. The development of a dedicated beamline for at-wavelength EUVL mask blank is well underway with design improvements to increase the sensitivity of the system and available beam flux.

ACKNOWLEDGMENTS

This work, performed at the LBNL, is supported by the Extreme Ultraviolet Limited Liability Company (EUV LLC) and by the Office of Energy Research, Basic Energy Sciences, of the U.S. Department of Energy under Contract No. DE-AC03-76SF00098. This research was jointly sponsored in part under SRC Contract No. 96-LC-460 and DARPA Grant No. MDA972-97-1-0010. The authors thank Jeff Mast at Lawrence Livermore National Laboratory for AFM measurements on the sample.

[1]See papers in *OSA TOPS on Extreme Ultraviolet Lithography*, edited by G. D. Kubiak and D. Kania (Optical Society of America, Washington, DC, 1996), Vol. 4.
[2]See special issue on Soft X-ray Projection Lithography, Appl. Opl., Dec. 1, 1993.
[3]K. Nguyen, A. MacDowell, K. Fujii, D. M. Tennant, and L. A. Fetter, in *OSA TOPS on Extreme Ultraviolet Lithography*, edited by G. D. Kubiak and D. Kania (Optical Society of America, Washington, DC, 1996), Vol. 4, p. 49.
[4]Y. Lin and J. Bokor, J. Vac. Sci. Technol. B **15**, 2467 (1997).
[5]S. P. Vernon, D. R. Kania, P. A. Kearney, R. A. Levesque, A. V. Hayes, B. Druz, E. Osten, R. Rajan, and H. Hedge, in *OSA TOPS on Extreme Ultraviolet Lithography*, edited by G. D. Kubiak and D. Kania (Optical Society of America, Washington, DC, 1996), Vol. 4.
[6]J. H. Underwood, in *OSA TOPS on Extreme Ultraviolet Lithography*, edited by G. D. Kubiak and D. Kania (Optical Society of America, Washington, DC, 1996), Vol. 4, p. 162.
[7]J. H. Underwood, E. M. Gullikson, M. Koike, P. J. Batson, P. E. Denham, K. D. Franck, R. E. Tackaberry, and W. F. Steele, Rev. Sci. Instrum. **67**, 1 (1996).
[8]P. Kirkpatrick and A. V. Baez, J. Opt. Soc. Am. **38**, 766 (1948).
[9]J. H. Underwood, Space Sci. Instrum. **3**, 259 (1977).
[10]See R. Hemphill, J. Edelstein, and D. Rogers, Appl. Opt. **36**, 1421 (1997), and references therein.